

# Geometric phase of light-induced conical intersections: Adiabatic time-dependent approach

Gábor J. Halász(1), Péter Badankó(2) and Ágnes Vibók(2),(3)\*,†

†(1)*Department of Information Technology, University of Debrecen, H-4002 Debrecen, PO Box 400, Hungary*

‡(2)*Department of Theoretical Physics, University of Debrecen, H-4002 Debrecen, PO Box 400, Hungary*

¶(3)*ELI-ALPS, ELI-HU Non-Profit Ltd, H-6720 Szeged, Dugonics tér 13, Hungary*

E-mail: vibok@phys.unideb.hu

## Abstract

Conical intersections are degeneracies between electronic states and are very common in nature. It has been found that they can also be created both by standing or by running laser waves. The latter are called light-induced conical intersections. It is well known that conical intersections are the sources for numerous topological effects which are manifested e.g. in the appearance of the geometric or Berry phase. In one of our former works by incorporating the diabatic-to-adiabatic transformation angle with the line-integral technique we have calculated the Berry-phase of the light-induced conical intersections.

Here we demonstrate that by using the time dependent adiabatic approach suggested by Berry the geometric phase of the light-induced conical intersections can also be obtained and the results are very similar to those of the time-independent calculations.

**Keywords:** Born-Oppenheimer approximation; Conical intersections; Light-induced conical intersections; Geometric phase;

## Introduction

Conical intersections (CIs) are degeneracies between two or more electronic states and play an important mechanistic role in the nonadiabatic dynamics of polyatomic molecules<sup>1-8</sup>. At the close vicinity of the CIs the Born-Oppenheimer adiabatic approximation<sup>1</sup> breaks down due to the strong nonadiabatic coupling between the nuclear and electronic motions. Several important photophysical and photochemical processes like dissociation, proton transfer, isomerization or radiationless deactivation of the excited states are associated with the appearance of CIs<sup>7</sup>. These degeneracies are not isolated, rather they are connected points forming a seam and can exist already between low lying states of triatomic molecule. In truly large molecular systems they are very abundant.

It is well-known that under “natural” (field-free) conditions CIs cannot be formed between different electronic states in diatomic molecules<sup>2</sup>. The one degree of freedom presents in these object is generally not enough to span a branching space and therefore only an avoided crossing result. However, applying standing<sup>9</sup> or running laser waves<sup>10</sup>, CIs can be created even in diatomics. In the first situation, the laser light induces CIs (“light-induced” conical intersections, LICIs) which couple the center of mass motion with the internal rovibrational degrees of freedom<sup>9</sup>. In the latter case, the rotational motion provides the missing degree of freedom allowing the formation of a LICl<sup>10</sup>.

Recently, several theoretical and experimental studies have demonstrated that similarly to the natural CIs the light-induced conical intersections have also significant impact on the different dynamical properties of molecules<sup>11-20</sup>. Among others it can strongly modify e. g. the spectra, the alignment, the dissociation probability or fragment angular distribution of molecules<sup>11-20</sup>. However, there are features in which the natural and light-induced CIs differ significantly. As long as the position of a natural CI and the strength of its nonadiabatic effects are inherent properties of the electronic states of a molecule and

are difficult to modify, the energetic and spatial positions of the LICl can be controlled by changing the parameter settings (intensity, frequency) of the laser light. This latter can open up a new direction in the field of molecular quantum control processes.

The nonadiabatic couplings can become extremely large at the close vicinity of the CIs. Numerous statical and dynamical nonadiabatic phenomena originate from the presence of a CI. Longuet-Higgins and Herzberg have demonstrated<sup>21,22</sup> that each real adiabatic electronic state changes sign when transported continuously along a closed path encircling the point of CI. Mead and Truhlar conjuncted this geometrical phase effect with the single electronic state problem<sup>23</sup> and Berry generalized the theory<sup>24</sup>, hence the name Berry phase. Making sure that the electronic wave function remains single valued one has to multiply it by a phase factor and, as a consequence of it, this new electronic eigenfunction, instead of being real, becomes complex. The fact that the electronic eigenfunctions are altered has a direct impact on the nuclear dynamics even if it happens in a single potential energy surface. Therefore having a nontrivial Berry phase in a molecular system can be seen as a direct fingerprint of the CI.

In the last three decades several works made remarkable contributions to the subject of molecular topological features<sup>25-50</sup>. However, all of these works related to the geometrical or topological properties, like Berry phase etc... of natural conical intersections.

In our earlier papers<sup>11,12</sup> we have calculated the Berry phase around the light-induced conical intersection formed in the Na<sub>2</sub> molecule in the presence of external electric field. Due to non vanishing transition dipole moment the 663 nm light can resonantly couple the  $X^1\Sigma_g^+$  and  $A^1\Sigma_u^+$  electronic states giving rise to a light-induced conical intersection. During the calculations  $2 \times 2$  Floquet form has been assumed for the Hamiltonian. Combining the calculation of adiabatic-to-diabatic transformation angle<sup>4-6,8</sup> with the time-independent line integral technique<sup>8</sup>, we could calculate the Berry phase for different close contours which either surrounded or not surrounded the LICl. Obtained results were similar to those calculated for CIs given in nature demonstrating that a “true” CI has been found.

In the present work we would like to go beyond the time-independent description.

Here we intend to provide calculations for the geometric phase of the light-induced conical intersection applying the time-dependent adiabatic approximation proposed by Berry in his famous work<sup>24</sup>. Our showcase example is the  $D_2^+$  molecule. We demonstrate that for certain initial conditions by assuming again  $2 \times 2$  Floquet form for the Hamiltonian the time-dependent description can provide similar results to the time-independent one.

The article is structured as follows. In the next section, our working Hamiltonian and the criteria for obtaining LICl are described. The applied method and the basic formulas, as well as the numerical procedures are briefly summarized in the third section. In the fourth section the numerical results are presented and discussed. Finally we present conclusions in Section five.

## The Hamiltonian

Let us define the Hamiltonian which governs the dynamics of the  $D_2^+$  molecule. Two electronic eigenstates  $V_1(R)$  (ground,  $1s\sigma_g$ ) and  $V_2(R)$  (excited,  $2p\sigma_u$ ) are included in the Hamiltonian which are coupled by a running laser wave (see in Figure 1). The non-vanishing transition dipole matrix element  $d(R) \left( = - \left\langle \Phi_1^e \left| \sum_j r_j \right| \Phi_2^e \right\rangle \right)$  is responsible for the light-induced electronic transition. The corresponding Born-Oppenheimer potentials and the transition dipole were taken from<sup>51,52</sup>. As the nuclear coordinate  $R$  and the molecular orientation  $\theta$  are taken as parameters during the calculations our Hamiltonian is defined by the potential energies and the laser-molecule interaction. This interaction is given in the dipole approximation as the scalar product of the transition dipole moment  $\vec{d}$  and the electric field vector  $\vec{\epsilon}$ :

$$\vec{d} \cdot \vec{\epsilon} = \epsilon_0 d(R) \cos \theta \cos(\omega_L t). \quad (1)$$

In Eq. (1)  $\epsilon_0$  is the maximum laser field amplitude,  $I_0$  ( $\sim \epsilon_0^2$ ) is the laser intensity,  $\theta$  denotes the angle between the polarization direction and the direction of the transition dipole  $d(R)$  and  $\omega_L$  is the laser frequency which couples the two electronic states at  $R = 5$  a.u. nuclear distance ( $\omega_L = 1.359 \text{ eV}$ ).

Let us represent the Hamiltonian in the Floquet picture. Therefore, the original Hamiltonian is transformed into an equivalent static problem by using the leading term in the Fourier series expansion of the solution of the time-dependent Schrödinger equation. Then the field-dressed form reads

$$\hat{\mathbf{H}} = \begin{pmatrix} V_1(R) & (\epsilon_0/2)d(R) \cos \theta \\ (\epsilon_0/2)d(R) \cos \theta & V_2(R) - \hbar\omega_L \end{pmatrix} \quad (2)$$

In this dressed state representation the interaction between the molecule and the electromagnetic field is obtained by shifting the energy of the excited potential curve by  $\hbar\omega_L$ . This picture is often used to explain various phenomena in the area of strong field physics whenever only net one-photon is absorbed by the molecule.

As a results of the dressed state representation a crossing is formed between the diabatic ground and the dressed excited potential energy curves. After diagonalizing the diabatic potential matrix Eq. 2, the resulting adiabatic or light-induced surfaces ( $V_{lower}$  and  $V_{upper}$ ) form a light-induced conical intersection (see in Figure 1) whenever the following conditions are fulfilled<sup>10,11</sup>:

$$\cos\theta = 0 \quad \left(\theta = \frac{\pi}{2}\right) \quad \text{and} \quad V_1(R) = V_2(R) - \hbar\omega_L. \quad (3)$$

An important feature of the light-induced conical intersections as compared to the natural CIs is that their fundamental characteristics can be modified by the external field. It has already been shown that the intensity of the field determines the strength of the nonadiabatic coupling, namely the steepness of the cone, while the energy of the field specifies the position of the LICl.

## The methodology and the numerical details

The main subject of this section is to obtain the appropriate expression so as to compute the geometric phase.

Let us consider again the working Hamiltonian Eq. 2 which is parametrized by  $R$  and  $\theta$ . If the system starts in an eigenstate  $\Phi(R, \theta)$  with an energy  $E(R, \theta)$ , then it evolves into the state  $\exp[-iE(R, \theta)t]\Phi(R, \theta)$ . Now let the parameters vary slowly,  $R = R(t)$  and  $\theta = \theta(t)$ <sup>1</sup>, then due to the adiabatic theorem, the eigenstates  $\Phi(R, \theta)$  are replaced by one of the actual eigenstates  $\Phi(R(t), \theta(t))$ . If both  $R(t)$  and  $\theta(t)$  are periodic functions of time with a period of  $T$  they describe a closed path in the configuration space. That is, for the time  $t = T$  the initial state  $\Phi(R(t=0), \theta(t=0))$  evolves into the final state which is identical with the initial state except for a phase factor:  $\Phi(R(T), \theta(T)) = \exp(i\chi) \cdot \Phi(R(0), \theta(0))$ . It is easy to see that the phase factor is identical with the autocorrelation function ( $C(t) = \langle \Phi(R(0), \theta(0)) | \Phi(R(t), \theta(t)) \rangle$ ) at time  $T$ . Berry showed<sup>24</sup> that  $\chi$  is the sum of  $\delta = -\int_0^T E(R(t'), \theta(t')) dt'$  and a quantity  $\gamma$ , latter is called the adiabatic phase. Here  $\chi$  and  $\delta$  are the overall and the dynamical phases, respectively.

Both the  $\chi$  and the  $\delta$  functions can be generalized for any arbitrary time  $t$ . To obtain the actual expressions for the  $\chi(t)$  and  $\delta(t)$  phases we refer to the work of Mukunda and Simon<sup>26</sup>. Among others they have pointed out that the overall phase is the argument of the autocorrelation function

$$\chi(t) = \arg \langle \Phi(R(0), \theta(0)) | \Phi(R(t), \theta(t)) \rangle \quad (4)$$

and the dynamical phase is as follows

$$\delta(t) = i \int_0^t \langle \Phi(R(t'), \theta(t')) | \dot{\Phi}(R(t'), \theta(t')) \rangle dt'. \quad (5)$$

Aharonov and Anandan<sup>25</sup> pointed out that  $\gamma$  is a purely geometrical property of the path which is parametrically defined by the functions  $R = R(t)$  and  $\theta = \theta(t)$  and can be calculated as the difference of the  $\chi(t)$  and  $\delta(t)$  at the end of the closed path. Therefore its value depends only upon the contour followed by the system in the configuration space. Hence the name of  $\gamma$  is geometric phase<sup>2</sup>. If  $\Phi(R(t), \theta(t))$  is the solution of the dynamical

---

<sup>1</sup>Here we allow a very slow time dependence of the  $R$  and  $\theta$  parameters, so as to assume an implicit adiabatic time dependence of the working Floquet Hamiltonian.

<sup>2</sup>From now on we will refer to  $\gamma$  as Berry, geometric or adiabatic phase.

Schrödinger equation, i.e., satisfies the  $i\hbar \left| \dot{\Phi}(R(t), \theta(t)) \right\rangle = \hat{H}(R(t), \theta(t)) |\Phi(R(t), \theta(t))\rangle$ , then we obtain for Eq. 5

$$\delta(t) = \frac{1}{\hbar} \int_0^t \left\langle \Phi(R(t'), \theta(t')) | \hat{H}(R(t), \theta(t)) | \Phi(R(t'), \theta(t')) \right\rangle dt'. \quad (6)$$

Using Eqs. 4 and 6 one can calculate the geometric phase  $\gamma$ , as difference of the  $\chi(t)$  and  $\delta(t)$  expressions at the end of the closed path for adiabatically slow changes of the parameters  $R(t)$  and  $\theta(t)$  over the whole path. As we do not know in advance how slow change can be considered as an adiabatic one during the numerical simulations we consider the quantity

$$\tilde{\gamma} = \chi(T) - \delta(T) \quad (7)$$

as an approximation for the Berry phase for the given contour.

To get the  $\Phi(R(t), \theta(t))$  wave function we have solved numerically the time-dependent Schrödinger equation by using implicit 4th order Runge-Kutta integrator with Gaussian points<sup>53</sup> implemented in the GNU Scientific Library<sup>54</sup>.

## Results and discussion

So as to understand the meaning of the numerical results to be presented in this paper, we first discuss the geometrical situation for which the above approach is applied and then analyze the numerical results.

The light-induced adiabatic states ( $V_{lower}$  and  $V_{upper}$ ) as well as the position of the corresponding light-induced conical intersection are displayed in Figure 1. The geometrical arrangement used as contours in the geometric phase calculations are shown in Figure 2. Here, four different ellipses are presented but only one of them surrounds the light-induced conical intersection. The numerical calculations take place along these closed paths characterized by their centers  $(R_c, \theta_c)$  and radii  $(\rho_R, \rho_\theta)$ . The actual position is

given by an angle  $\beta(t) = \beta_0 + t/T \cdot 2\pi$ :

$$\begin{aligned} R(t) &= R_c + \rho_R \cos \beta(t) \\ \theta(t) &= \theta_c - \rho_\theta \sin \beta(t). \end{aligned} \tag{8}$$

The applied parameters for the different contours are displayed in Table 1. In Table 2 the obtained approximated values ( $\tilde{\gamma}$ ) for the geometric phase  $\gamma$  are presented (in unit of  $\pi$ ) for the contour  $\mathcal{C}_1$  which encircles the LICI with the initial wave function chosen to be the lower lying eigenstate of the Hamiltonian Eq. 2 at point  $S_1$ . The approximation is based on the difference of the argument of the autocorrelation function (Eq. 4) and the dynamical phase (Eq. 6) at the end of the path (see Eq. 7). The applied photon energy is  $\hbar\omega_L = 1.359 \text{ eV}$ . In the rows of Table 2 the different field intensities are chosen to be between  $I = 1 \times 10^{10} \frac{W}{\text{cm}^2}$  and  $I = 1 \times 10^{15} \frac{W}{\text{cm}^2}$ . In the columns, the periodic times of the round transport of the ellipse are indicated as a unit of the periodic time of the laser pulse ( $\frac{2\pi}{\omega_L}$ ). The larger the value of  $T$  indicated here, the more adiabatic the process of encircling the ellipse. As the contour  $\mathcal{C}_1$  surrounds only a single conical intersection the value of the geometric phase  $\gamma$  is expected to be  $\pm\pi$  and so for long enough  $T$  values  $\tilde{\gamma}$  should be in the close vicinity of  $(2n + 1)\pi$  (where  $n$  is an integer). We can observe in Table 2 that except for the lowest studied intensities the value of  $\tilde{\gamma}$  is really close to  $\pi$ , whenever  $T \geq 500 \times \frac{2\pi}{\omega_L}$ . The numerical problem at small intensities are related to the fact that for the field free case (zero intensity) the value of  $\gamma$  should be zero. As a consequence, in weak fields we need extremely slow surrounding of the contour to be able to consider it as an adiabatic one. For the extremely large values of  $T$  question arises about the accuracy concerning the numerical integration of the Schrödinger equation. As a simple check for this issue we have also performed numerical integration over the same contour for the field free case. The obtained  $\tilde{\gamma}$  values are displayed in the first row of Table 2. All of these values are close to the expected value of  $\gamma = 0$ .

For larger intensities the adiabatic region can be reached before  $T = 500 \times \frac{2\pi}{\omega_L}$ . Table 2 shows that for intensities larger than  $I = 1 \times 10^{13} \frac{W}{\text{cm}^2}$  the beginning of this adiabatic



region is moving towards larger values of  $T$  with the increasing intensities. This effect is related to the fact that at higher intensities the derivative of the adiabatic potentials ( $V_{lower}$  and  $V_{upper}$ ) respect to the position on the contour (controlled by parameter  $\beta(t)$ ) become significantly larger than the same derivatives of the diabatic ones. As a result, slower change is requested in the value of the  $\beta(t)$  parameter so as to consider the process being adiabatic.

In Figure 3 the difference of the  $\chi(t)$  and  $\delta(t)$  functions are displayed as a function of time with three different time resolutions. Results are presented of the set of simulations for which the  $\tilde{\gamma}$  values are displayed in Table 2 at  $I = 1 \times 10^{13} \frac{W}{cm^2}$  field intensity. It can be seen that the different curves display different shapes at  $t/T = 0.5$ , but all of them possess relatively sudden jumps ranging from near zero to close to the final value. The phase jumps always take place at that position of  $t/T$ , where the value of the autocorrelation function tends to zero. In the panels of Figure 3 the positions of the phase jumps are always positioned at  $t/T = 0.5$ . But this happens due to symmetry reasons. In the current geometrical arrangement (see on Figure 2), the center of the ellipse is also the position of the LICl. In this situation, four symmetry points can be considered concerning the starting position of the encircling of the ellipse. These symmetry points are the endpoints of the small and the large axes of the ellipse. If one starts to circle the ellipse at one of these points the phase jumps always occur at  $t/T = 0.5$ . If this process starts from a different point then the phase jump happens at another value of  $t/T$ . E.g. for the contour  $\mathcal{C}_1$  the phase jump occurs at  $t/T = 0.5$  if the starting points are  $S_1$  or  $S'_1$  but for starting point  $S''_1$  the jump happens at  $t/T \cong 0.44$ . Nevertheless, the values of the phase jumps are always very close to an odd multiple of  $\pi$ . The longer the encircling time, the steeper the phase jump, but its value is getting closer and closer to the final value of  $\tilde{\gamma}$ . This effect is clearly recognizable as long as the time resolution gets finer (see on panels of Figure 3).

We have also computed the value of the approximate geometric phase  $\tilde{\gamma}$  along those ellipses which do not surround LICl. Obtained results are always very close to zero.

For completeness we have performed similar calculations on the upper adiabatic sur-

faces as well. All of these calculations provide the same results as for the case of lower surface but always with an opposite sign for  $\tilde{\gamma}$ . Table 3 displays some values of  $\tilde{\gamma}$  at  $I = 1 \times 10^{13} \frac{W}{cm^2}$  field intensity. We notice that for contour  $\mathcal{C}_1$  starting the simulation at point  $S'_1$  the calculated values of  $\tilde{\gamma}$  are always around of  $\pm 3\pi$  or  $\pm 5\pi$  depending upon the actual speed of the surrounding. (All of these values are odd multiples of  $\pi$  so they are in agreement with the expected value of the geometric phase  $\gamma = \pi$ .) This uncertainty is clearly related to the fact that the correct value of the autocorrelation function is zero at  $t/T = 0.5$  and therefore it is extremely hard to follow its argument during the numerical simulations.

## Conclusions

By applying adiabatic time-dependent framework and Floquet representation for the Hamiltonian we have calculated the geometric phase of the light-induced conical intersection formed in the  $D_2^+$  molecule. It has been demonstrated that assuming certain conditions for the initial wave functions the adiabatic time-dependent results for the geometric phase are similar to those obtained from the time-independent solutions<sup>11,12</sup>. Obviously, obtained numerical results are also in full agreement with the values of the Berry phase that hold for the natural conical intersections.

In the future, our aim is to compute the Berry phase for the exact time-dependent light-matter Hamiltonian, too. However, this is not an easy task because of the explicit time-dependence of the Hamiltonian. The latter gives rise to additional difficulties and the adiabatic transport round a close path is far from being trivial.

## Acknowledgements

The supercomputing service of NIF has been used for this work. This research was supported by the EU-funded Hungarian grant EFOP-3.6.2-16-2017-00005. The authors thank Tamás Vértési for many fruitful discussions.

Table 1: Parameters of the applied contours in the configuration space corresponding to Figure 2 and Eq. 8.

Contour	$R_c$ [a.u.]	$R_\theta$ [rad]	$\rho_c$ [a.u.]	$\rho_\theta$ [rad]	$\beta_0$ [rad]
$\mathcal{C}_1$	5	$\pi/2$	1	$\pi/3$	$-\pi/2$ for $S_1$ ; 0 for $S'_1$ ; $-\pi/4$ for $S''_1$
$\mathcal{C}_2$	7	$\pi/2$	1	$\pi/3$	$-\pi/2$ for $S_2$
$\mathcal{C}_3$	3	$\pi/2$	1	$\pi/3$	$-\pi/2$ for $S_3$
$\mathcal{C}_4$	5	$\pi/5$	1	$\pi/6$	$-\pi/2$ for $S_4$

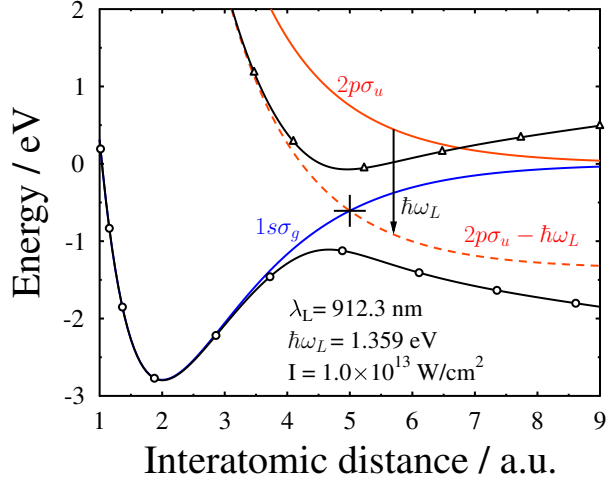


Figure 1: A cut through the potential energy surface of the  $D_2^+$  molecule as a function of interatomic separation. Diabatic energies of the ground  $V_1(R)$  ( $1s\sigma_g$ ) and the first excited  $V_2(R)$  ( $2p\sigma_u$ ) states are displayed with solid blue and red lines, respectively. The field dressed excited state ( $2p\sigma_u - \hbar\omega_L$ ; dashed red line) forms a light induced conical intersection (LICI) with the ground state. For the case of a laser frequency  $\hbar\omega_L = 1.359\text{eV}$  and field intensity of  $1 \times 10^{13} \frac{\text{W}}{\text{cm}^2}$  a cut through the adiabatic surfaces at  $\theta = 0$  (parallel to the field) is also shown by solid black lines marked with circles ( $V_{lower}$ ) and triangles ( $V_{upper}$ ). We denote with a cross the position of the LICI ( $R_{LICI} = 5.00 \text{ a.u.}$ ).

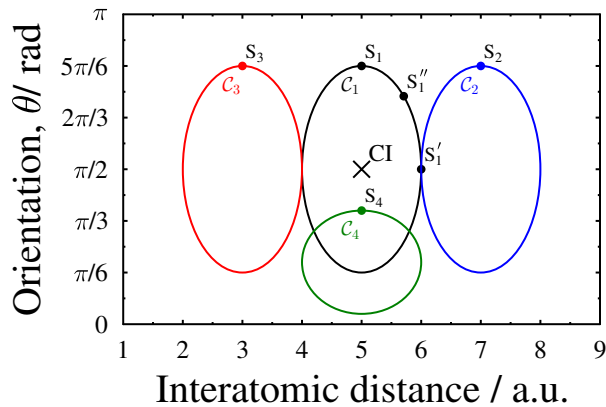


Figure 2: Geometrical arrangement of the contours used in the geometrical phase calculations. Four different geometrical arrangements are applied and only one curve surrounds the LICI. The black cross shows the position of the LICI. Dots denote the starting points of the different simulations in the configuration space.

Table 2: The difference of the total and dynamical phases in the units of  $\pi$  at the end of the paths ( $t = T$ )  $\mathcal{C}_1$  surrounding the LICI (see on Fig.2) The starting point of the surrounding is  $S_1$  and the initial wave function is chosen to be on the lower adiabatic surface.

Intensity [ $W/cm^2$ ]	$T$ [ $2\pi/\omega_L$ ]					
	10	20	50	100	200	500
field free	$<1 \cdot 10^{-6}$	$<1 \cdot 10^{-6}$	$<1 \cdot 10^{-6}$	$<1 \cdot 10^{-6}$	$<1 \cdot 10^{-6}$	$<1 \cdot 10^{-6}$
$1 \cdot 10^{10}$	0.4465	-8.2194	0.0682	13.7408	-75.0925	32.9789
$3 \cdot 10^{10}$	0.0663	-7.7439	-3.7613	8.8010	-29.9996	-29.6432
$5 \cdot 10^{10}$	-0.1732	-7.4972	-5.1357	4.5659	-24.4448	-96.5521
$1 \cdot 10^{11}$	-0.5458	-7.2619	-3.5758	7.7951	-51.2940	-17.0145
$3 \cdot 10^{11}$	-0.9243	2.2194	-9.2701	-1.6251	-4.4822	-0.4876
$5 \cdot 10^{11}$	-0.6192	1.9429	-0.6340	-3.7004	-0.4275	0.4730
$1 \cdot 10^{12}$	1.1093	-4.9457	-1.3928	0.2718	0.6346	0.8578
$3 \cdot 10^{12}$	0.3088	0.3741	0.7764	0.8911	0.9463	0.9785
$5 \cdot 10^{12}$	0.4448	0.7695	0.8962	0.9479	0.9741	0.9896
$1 \cdot 10^{13}$	0.7615	0.8417	0.9481	0.9741	0.9871	0.9948
$3 \cdot 10^{13}$	5.4996	2.6332	0.9582	0.9795	0.9898	0.9959
$5 \cdot 10^{13}$	7.7773	11.9147	2.9448	0.9765	0.9883	0.9953
$1 \cdot 10^{14}$	8.1765	21.4233	14.7622	0.9681	0.9846	0.9939
$3 \cdot 10^{14}$	9.4209	35.7743	104.6614	54.7573	2.9740	0.9897
$5 \cdot 10^{14}$	5.2325	35.7902	146.1297	199.6102	20.9600	0.9868
$1 \cdot 10^{15}$	0.6056	37.9231	190.5541	418.5138	252.6389	0.9814

Intensity [ $W/cm^2$ ]	$T$ [ $2\pi/\omega_L$ ]					
	1000	2000	5000	10000	20000	50000
field free	$1 \cdot 10^{-6}$	$2 \cdot 10^{-6}$	$4 \cdot 10^{-6}$	$8 \cdot 10^{-6}$	$15 \cdot 10^{-6}$	$24 \cdot 10^{-6}$
$1 \cdot 10^{10}$	-305.7453	-82.5002	-192.7763	-60.5332	-29.1699	-10.6957
$3 \cdot 10^{10}$	-148.5720	-49.4776	-12.8597	-5.5952	-2.2615	-0.3007
$5 \cdot 10^{10}$	-39.6079	-13.1177	-3.8062	-1.3639	-0.1775	0.5295
$1 \cdot 10^{11}$	-5.7173	-2.0801	-0.1961	0.4041	0.7023	0.8809
$3 \cdot 10^{11}$	0.3002	0.6534	0.8618	0.9309	0.9655	0.9862
$5 \cdot 10^{11}$	0.7400	0.8705	0.9483	0.9741	0.9870	0.9948
$1 \cdot 10^{12}$	0.9293	0.9646	0.9859	0.9929	0.9964	0.9986
$3 \cdot 10^{12}$	0.9893	0.9946	0.9978	0.9989	0.9994	0.9998
$5 \cdot 10^{12}$	0.9948	0.9974	0.9990	0.9995	0.9997	0.9999
$1 \cdot 10^{13}$	0.9974	0.9987	0.9995	0.9997	0.9999	0.9999
$3 \cdot 10^{13}$	0.9980	0.9990	0.9996	0.9998	0.9999	1.0000
$5 \cdot 10^{13}$	0.9977	0.9988	0.9995	0.9998	0.9999	1.0000
$1 \cdot 10^{14}$	0.9969	0.9985	0.9994	0.9997	0.9998	1.0000
$3 \cdot 10^{14}$	0.9949	0.9974	0.9990	0.9995	0.9997	1.0000
$5 \cdot 10^{14}$	0.9934	0.9967	0.9987	0.9993	0.9997	1.0001
$1 \cdot 10^{15}$	0.9907	0.9954	0.9981	0.9990	0.9995	1.0003

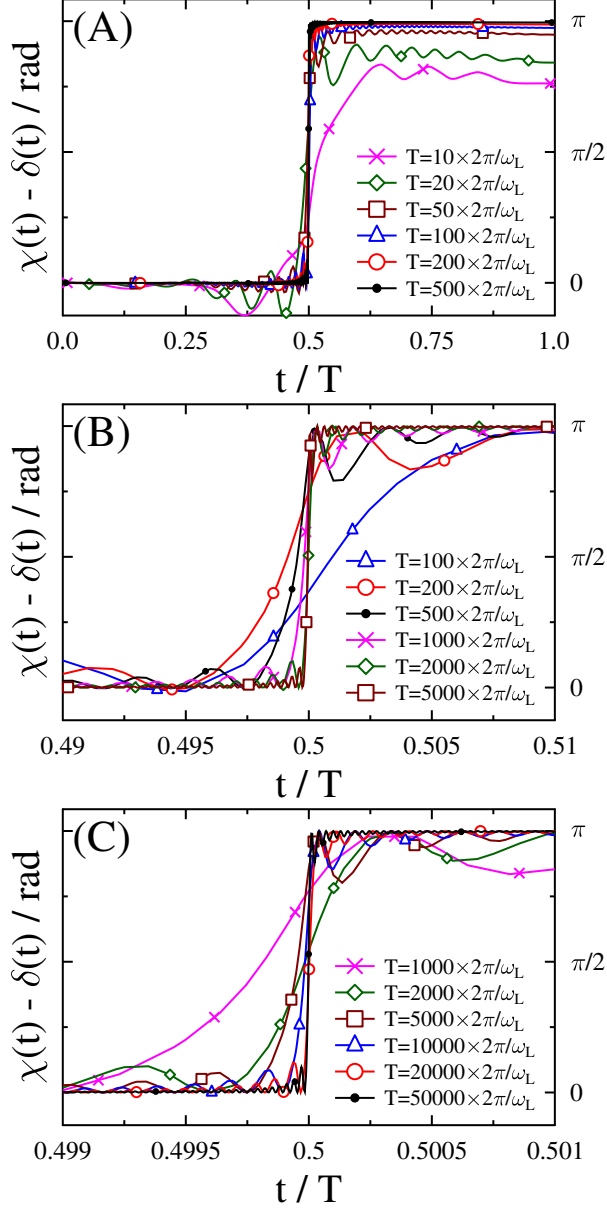


Figure 3: The difference of the total and the dynamical phases as a function of time. This quantity provides the value of the geometric phase  $\gamma$  at  $t/T = 1$  if the  $T$  is long enough.  $T$  is the periodic time encircling the ellipse. The computation starts at the point  $S_1$  of the ellipse which surrounds the LIC1 (see on Fig.2). Different time intervals are depicted. In panel (A) the whole time period  $t/T \{0, \dots, 1\}$ , in panel (B) the  $t/T \{0.49, \dots, 0.51\}$  and in panel (C) the  $t/T \{0.499 \dots 0.501\}$  are figured. The applied intensity is  $I = 1 \times 10^{13} \frac{W}{cm^2}$ .

## References

- (1) M. Born, Ann. Phys. **84**, 457 (1927).
- (2) J. von Neumann and E. P. Wigner, Zeit. fur Phys. **30**, 467 (1929).
- (3) Y. Aharonov, and D. Bohm, Phys. Rev. **115**, 485 (1959).
- (4) H. Köppel, W. Domcke, and L. S. Cederbaum, Adv. Chem. Phys. **57**, 59 (1984).
- (5) M. Baer, Phys. Rep. **358**, 75 (2002).
- (6) G. A. Worth and L. S. Cederbaum, Ann. Rev. Phys. Chem. **55**, 127 (2004).
- (7) W. Domcke, D. R. Yarkony and H. Köppel, *Conical Intersections: Electronic Structure, Dynamics and Spectroscopy*; World Scientific: Singapore; 2004.
- (8) Press, Oxford, UK, 1954. M. Baer, Beyond Born Oppenheimer: Electronic Non-Adiabatic Coupling Terms and Conical Intersections, Wiley, Hoboken, NJ, 2006.
- (9) N. Moiseyev, M. Sindelka, and L. S. Cederbaum, J. Phys. B **41**, 221001 (2008).
- (10) M. Sindelka, N. Moiseyev, and L. S. Cederbaum, J. Phys. B **44**, 045603 (2011).
- (11) G. J. Halász, Á. Vibók, M. Sindelka, N. Moiseyev, and L. S. Cederbaum, J. Phys. B **44**, 175102 (2011).
- (12) G. J. Halász, M. Sindelka, N. Moiseyev, L. S. Cederbaum, and Á. Vibók, J. Phys. Chem. A. **116**, 2636 (2012).
- (13) G. J. Halász, Á. Vibók, N. Moiseyev, and L.S. Cederbaum, J. Phys. B **45**, 135101 (2012).
- (14) G. J. Halász, A. Csehi, Á. Vibók, and L. S. Cederbaum, J. Phys. Chem. A **118**, 11908 (2014).
- (15) G.J. Halász, Á. Vibók, and L.S. Cederbaum, J. Phys. Chem. Lett. **6**, 348 (2015).
- (16) M. Pawlak, and N. Moiseyev Phys. Rev. A **92**, 023403 (2015).

- (17) A. Csehi, G. J. Halász, L. S. Cederbaum, and Á. Vibók, *Faraday Discuss.* **194**, 479 (2016).
- (18) A. Csehi, G. J. Halász, L. S. Cederbaum and Á. Vibók, *J. Phys. Chem. Lett.* **8**, 1624 (2017).
- (19) M. E. Corrales, J. González-Vázquez, G. Balerdi, I. R. Solá, R. de Nalda, and L. Bañares, *Nature Chem.* **6**, 785 (2014).
- (20) A. Natan, M. R. Ware, V. S. Prabhudesai, U. Lev, B. D. Bruner, O. Heber, and P. H. Bucksbaum, *Phys. Rev. Lett.* **116**, 143004 (2016).
- (21) G. Herzberg, H. C. Longuet-Higgins, *Discuss. Faraday Soc.* **35**, 77 (1963).
- (22) H. C. Longuet-Higgins, *Proc. Roy. Soc. (London) A* **344**, 147 (1975).
- (23) C. A. Mead and D. G. Truhlar, *J. Chem. Phys.* **70**, 2284 (1979).
- (24) M. V. Berry, *Proc. Roy. Soc. (London) A* **392**, 45 (1984).
- (25) Y. Aharonov, and J. Anandan, *Phys. Rev. Lett.* **58**, 1593 (1987).
- (26) N. Mukunda, R. Simon, *Ann. Phys. (N.Y.)* **228**, 205 (1993).
- (27) M. Baer and R. Englman, *Chem. Phys. Lett.* **265**, 105 (1997).
- (28) M. Baer, A. Yahalom, and R. Englman, *J. Chem. Phys.* **109**, 6550 (1998).
- (29) R. Englman and M. Baer, *J. Phys.: Cond. Matt.* **11**, 1059 (1999).
- (30) R. Englman and A. Yahalom, *Phys. Rev. A* **67**, 054103 (2003).
- (31) R. Englman and A. Yahalom, *Phys. Rev. B* **69**, 224302 (2004).
- (32) R. Englman, *Chem. Phys. Lett.* **635**, 224 (2015).
- (33) E. Sjöqvist, *Int. J. Quant. Chem.* **115**, 1311 (2015).
- (34) D. J. Moore, *J. Phys. A* **23**, L665 (1990).

- (35) D. J. Moore, Di, J. Phys. A **23**, 5523 (1990).
- (36) D. J. Moore, Phys. Rep. **210**, 1 (1991).
- (37) B. Kendrick, Phys. Rev. Lett. **79**, 2431 (1997).
- (38) D. Xiao, M.-C. Chang, and Q. Niu, Rev. Mod. Phys. **82**, 1959 (2010).
- (39) I. G. Ryabinkin and A. F. Izmaylov, Phys. Rev. Lett. **111**, 220406 (2013).
- (40) L. Joubert-Doriol, I. G. Ryabinkin, and A. F. Izmaylov, J. Chem. Phys. **139**, 234103 (2013).
- (41) S. Henshaw, A.F. Izmaylov, arXiv:1710.08981, (2017).
- (42) S. K. Min, A. Abedi, K. S. Kim, and E. K. U. Gross, Phys. Rev.Lett. **113**, 263004 (2014).
- (43) R. Requist, F. Tandetzky, and E. K. U. Gross, Phys. Rev. A **93**, 042108 (2016).
- (44) A. Scherrer, F. Agostini, D. Sebastiani, E.K. U. Gross, and R. Vuilleumier, Phys. Rev. X **7**, 031035 (2017).
- (45) F.E. Curchod Basile, and F. Agostini, J. Phys. Chem. Lett. **8**, 831, (2017).
- (46) M. Wang, L.F. Wei, and J.Q. Liang, Phys. Lett. A **379**, 1087 (2015).
- (47) C. Xie, J. Ma, X. Zhu, D.R. Yarkony, D. Xie, H. Guo, J. Am. Chem. Soc. **138**, 7828 (2016).
- (48) C. Xie, B. K. Kendrick, D. R. Yarkony, and H. Guo, J. Chem. Theory Comput. **13**, 1902 (2017).
- (49) C. Xie, D. R. Yarkony, and H. Guo, Phys. Rev. A **95**, 022104 (2017).
- (50) C. Xie and H. Guo, Chem. Phys. Lett. **683**, 222 (2017).
- (51) S. I. Chu, C. Laughlin, and K. Datta, Chem. Phys. Lett. **98**, 476 (1983).
- (52) F. V. Bunkin and I. I. Tugov, Phys. Rev. A **8**, 601 (1973).



- (53) Ascher, U.M., Petzold, L.R., Computer methods for ordinary differential and differential-algebraic equations, SIAM, Philadelphia, 1998. ISBN 0898714125, 9780898714128.
- (54) M. Galassi et al, GNU Scientific Library Reference Manual (3rd Ed.), ISBN 0954612078.

Table 3: The difference of the total and dynamical phases in the units of  $\pi$  at the end of the paths ( $t = T$ ). Different contours and initial wave functions are applied at  $I = 1 \times 10^{13} \frac{W}{cm^2}$ .

Contour/ Surface	$T [2\pi/\omega_L]$						
	500	1000	2000	5000	10000	20000	50000
$\mathcal{C}_1-S_1/$ lower	+0.99483	+0.99741	+0.99871	+0.99948	+0.99973	+0.99985	+0.99993
$\mathcal{C}_1-S_1/$ upper	-0.99483	-0.99742	-0.99871	-0.99948	-0.99974	-0.99987	-0.99995
$\mathcal{C}_1-S'_1/$ lower	+4.98611	+2.99305	+2.99652	+4.99859	+4.99926	+2.99957	+4.99965
$\mathcal{C}_1-S'_1/$ upper	-4.98611	-2.99306	-2.99653	-4.99861	-4.99931	-2.99966	-4.99987
$\mathcal{C}_1-S''_1/$ lower	+0.99483	+0.99741	+0.99871	+0.99948	+0.99973	+0.99985	+0.99993
$\mathcal{C}_1-S''_1/$ upper	-0.99483	-0.99742	-0.99871	-0.99948	-0.99974	-0.99987	-0.99995
$\mathcal{C}_2-S_2/$ lower	-0.00185	-0.00093	-0.00047	-0.00019	-0.00011	-0.00007	-0.00002
$\mathcal{C}_2-S_2/$ upper	+0.00185	+0.00092	+0.00046	+0.00019	+0.00009	+0.00005	+0.00002
$\mathcal{C}_3-S_3/$ lower	-0.00009	-0.00005	-0.00003	-0.00002	-0.00002	-0.00003	-0.00006
$\mathcal{C}_3-S_3/$ upper	+0.00009	+0.00005	+0.00003	+0.00003	+0.00003	+0.00001	+0.00026
$\mathcal{C}_4-S_4/$ lower	-0.04279	-0.02138	-0.01069	-0.00428	-0.00215	-0.00109	-0.00044
$\mathcal{C}_4-S_4/$ upper	+0.04279	+0.02138	+0.01069	+0.00428	+0.00214	+0.00107	+0.00043